Mol. Cells *34*, 407-412, October 31, 2012
DOI/10.1007/s10059-012-0198-8
pISSN: 1016-8478 eISSN: 0219-1032

Molecules and Cells
http://molcells.org

Crystal Structure of Pyridoxal Biosynthesis Lyase PdxS from *Pyrococcus horikoshii*

Atsushi Matsuura[1,5], Ji Young Yoon[2,5], Hye-Jin Yoon[2,5], Hyung Ho Lee[1,3,*], and Se Won Suh[2,4,*]

Pyridoxal 5′-phosphate (PLP) is the biologically active form of vitamin B_6 and is de novo synthesized from three substrates, dihydroxyacetone phosphate (DHAP), riburose 5-phosphate (RBP), and ammonia hydrolysed from glutamine. Glutamine amidotransferase (PdxT) catalyzes the production of ammonia from glutamine, while PdxS catalyzes the following condensation of ribulose 5-phosphate (Ru5P), glyceraldehyde-3-phosphate (G3P), and ammonia. PdxS exists as a hexamer or dodecamer depending on species and makes a 1:1 complex with PdxT. *Pyrococcus horikoshii* PdxS has a 37 amino acids insertion region, which is found in some archaeal PdxS proteins, but its structure and function are unknown. To provide further structural information on the role of the insertion region, the oligomeric state, and ligand binding mode of *P. horikoshii* PdxS, the crystal structure of PdxS from *P. horikoshii* was solved in two forms: (i) apo form, (ii) ribose 5-phosphate (R5P) complex and the quaternary structure of PdxS in solution was determined by analytical gel filtration. *P. horikoshii* PdxS forms hexamer in solution based on analytical gel filtration data. When we superimpose the structure of *P. horikoshii* PdxS with other dodecamer structures of PdxS, the additional insertion is located apart from the active site and induces a steric clash on the hexamer-hexamer interface of PdxS proteins. Our results suggest that the additional insertion perturbs dodecamer formation of *P. horikoshii* PdxS.

INTRODUCTION

Vitamin B_6 is an essential organic cofactor for a variety of enzymes, and is required for the maintenance of the nervous and immune systems in animals and humans (Bender, 1989); it also plays an important role as an antioxidant in various organisms (Chung et al., 1999; Ehrenshaft et al., 1999). Pyridoxal 5′-phosphate (PLP) is the biologically active form of vitamin B_6 and is essential for numerous enzyme reactions, including transamination, decarboxylation, racemization, and elimination in amino acid metabolism, biosynthesis of antibiotics, and DNA biosynthesis (Eliot and Kirsch, 2004; Percudani and Peracchi, 2003). As de novo PLP biosynthesis pathways exist in bacteria, fungi, protozoa, and plants, but are missing in mammals, PLP biosynthesis could be a target for developing antibiotics (Belitsky, 2004; Dong et al., 2004; Osmani et al., 1999). There are two mutually exclusive de novo pathways (deoxyxylulose 5′-phosphate (DXP)-dependent and DXP-independent) (Fitzpatrick et al., 2007; Tambasco-Studart et al., 2005). The DXP-dependent pathway exists in many eubacteria and produces PLP from erythrose 4-phosphate and 1-deoxy-D-xylulose 5-phosphate (Cane et al., 1999; Laber et al., 1999). In the DXP-independent pathway, which is employed in eubacteria, archaea, fungi, plants, plasmodia, and some metazoa, PLP is synthesized from dihydroxyacetone phosphate (DHAP) or its isomer glyceraldehyde 3-phosphate (G3P), ribose 5-phosphate (R5P) or its isomer ribulose 5-phosphate (RBP), and ammonia, which is formed by the hydrolysis of glutamine. The DXP-independent pathway involves the interplay of a synthase (PdxS) and a glutaminase (PdxT) displaying glutamine amidotransferase activity.

Crystal structures of PdxS (and PdxS homologs Pdx1, YaaD, and Snz1) and PdxT (and PdxT homologs Pdx2, YaaE, and Sno1) have been reported. PdxS from *Geobacillus stearothermophilus* is a cylindrical dodecamer consisting of a $(\beta/\alpha)_8$- or TIM-barrel fold (Zhu et al., 2005). The active site of *G. stearothermophilus* PdxS, a pair of hexameric rings, is positioned on the inside of the dodecamer (Zhu et al., 2005). The crystal structures of *Thermotoga maritima* YaaD-YaaE complex bound with RBP and the *Bacillus subtilis* Pdx1-Pdx2 complex have also been reported (Strohmeier et al., 2006; Zein et al., 2006). Both Pdx1-Pdx2 and YaaD-YaaE complexes are made up of 24 subunits consisting of a dodecameric Pdx1 (or YaaD) and Pdx2 (or YaaE) (Strohmeier et al., 2006; Zein et al., 2006). The glutaminase PdxT (Pdx2, YaaE) is inactive in the absence of the synthase subunit PdxS (Strohmeier et al., 2006; Zein et al., 2006; Zhu et al., 2005). The structure suggests that an oxyanion hole is formed in the active site of PdxT triggered by a peptide flip induced by interaction with PdxS (Strohmeier et al., 2006). The ammonia produced from the hydrolysis of glutamine

[1]Department of Bio & Nano Chemistry, Kookmin University, Seoul 136-702, Korea, [2]Department of Chemistry, College of Natural Sciences, Seoul National University, Seoul 151-742, Korea, [3]Department of Integrative Biomedical Science and Engineering, Kookmin University, Seoul 136-702, Korea, [4]Department of Biophysics and Chemical Biology, College of Natural Sciences, Seoul National University, Seoul 151-742, Korea, [5]These authors contributed equally to this work.
*Correspondence: sewonsuh@snu.ac.kr (SWS); hhlee@kookmin.ac.kr (HHL)

Received August 2, 2012; revised September 4, 2012; accepted September 6, 2012; published online October 18, 2012

Keywords: pdxS, pyridoxal biosynthesis lyase, pyridoxal 5'-phosphate (PLP), *Pyrococcus horikoshii*

Springer

by PdxT travels through an internal tunnel in the PdxS to reach the active site (Strohmeier et al., 2006). The crystal structures of *Saccharomyces cerevisiae* Snz1 (apo-, Snz1-G3P complex, and Snz1-PLP complex) have also been reported (Zhang et al., 2010). Recently, an electron microscopy analysis showed that *Plasmodium falciparum* PLP synthase organizes in fibers. An insertion in the *P. falciparum* Pdx2 could mediate intermolecular interactions in the fibers (Guedez et al., 2012).

The oligomeric nature of several PdxS proteins in solution has been characterized by analytical gel filtration or analytical ultracentrifugation. *B. subtilis* Pdx1 and *G. stearothermophilus* PdxS proteins have been shown to exist as a hexamer-dodecamer equilibrium in solution (Strohmeier et al., 2006; Zhu et al., 2005). Hexamer-dodecamer equilibrium in *G. stearothermophilus* PdxS was dependent on the salt concentration (Zhu et al., 2005). Sulfate ions form salt bridges with conserved residues (His115, Arg137, Arg138, and Lys187) on the hexamer-hexamer interface of *G. stearothermophilus* PdxS to help form a dodecamer (Zhu et al., 2005). *S. cerevisiae* Snz1 exists in a hexameric form in the crystal and solution (Neuwirth et al., 2009). A small insertion (Lys177) in *S. cerevisiae* Snz1 on the hexamer-hexamer interface is responsible for a shift from dodecamer to hexamer (Neuwirth et al., 2009). Notably, a long insertion, of 37 amino acids, is found in PdxS proteins of some archaea, including *Pyrococcus horikoshii* and *Methanococcus jannaschii*, but its structure and function are unknown.

To provide further structural information on this additional insertion, the oligomeric state, and the ligand binding mode of *P. horikoshii* PdxS, its crystal structure was solved in two forms, (i) the apo form, and (ii) the R5P complex form, and the quaternary structure of *P. horikoshii* PdxS in solution was determined by analytical gel filtration. R5P binds to the active site in a similar manner to R5P in the crystal structure of *Plasmodium berghei* Pdx1. Analytical gel filtration data demonstrated that *P. horikoshii* PdxS forms hexamers in solution. When we superimposed the structure of *P. horikoshii* PdxS on other dodecameric PdxS proteins, the additional insertion was located away from the active site and appeared to perturb dodecamer formation. The new structural information reported in this study will supplement the existing structural data regarding PdxS oligomerization and R5P recognition.

MATERIALS AND METHODS

Protein expression, purification, and crystallization

Methods of protein expression, purification, crystallization, and data collection are essentially the same as those previously published (Yoon et al, 2012). Briefly, PdxS from *P. horikoshii* was overexpressed in *Escherichia coli* strain Rosetta2 (DE3) pLysS and crystallized at 296 K using 2-methyl-2,4-pentanediol as a precipitant. The crystals grew to dimensions of 0.18 × 0.18 × 0.08 mm within 2 weeks. Crystals of apo and R5P complex forms of *P. horikoshii* PdxS diffracted to 2.7 Å and 3.1 Å resolution, respectively, and belonged to the monoclinic space group $P2_1$, with unit cell parameters of a = 59.30 Å, b = 178.56 Å, c = 109.23 Å, β = 102.97°, and a = 59.16 Å, b = 179.17 Å, c = 109.52 Å, β = 102.51°, respectively. The crystals of the R5P complex were obtained by soaking crystals of the apo protein in 50 mM R5P solution (100 mM imidazole, pH 8.0, 35% (v/v) 2-methyl-2,4-pentanediol, and 200 mM $MgCl_2$) for 3 min.

Structure determination and refinement

The structure was solved by the molecular replacement method using the hexameric form of *G. stearothermophilus* PdxS (PDB ID: 1ZNN) as the probe (Zhu et al., 2005). A cross-rotation search followed by a translation search was performed using the CNS program (Brünger et al., 1998). Subsequent manual model building was performed using the program O (Jones et al., 1991). The model was refined using CNS, and several rounds of model building, simulated annealing, positional refinement, and individual *B*-factor refinement were performed as those previously published (Lee, 2012; Yoon et al., 2011). The non-crystallographic symmetry restraints were relaxed in successive rounds of refinement. Water molecules were added using the CNS program, followed by a visual inspection, positional refinement, and *B*-factor refinement. The atomic coordinates and the structure factors were deposited in the Protein Data Bank (Accession codes 4FIQ and 4FIR for apo and R5P complex forms, respectively).

Analytical gel filtration

The purified *P. horikoshii* PdxS protein was subjected to analytical gel filtration chromatography on a Superdex 200 (10/300) column with the running buffer (50 mM Tris-HCl at pH 7.9 containing 200 mM NaCl) at a constant flow rate of 1 ml/min. The standard curve was obtained using molecular weight markers (Sigma, catalog no. MWGF1000-1KT). The Stokes radii of apoferritin, β-amylase, alcohol dehydrogenase, albumin, and carbonic anhydrase were calculated from the crystal structure (PDB IDs: 2W0O**,** 1FA2, 2HCY, 3V03, 1V9E, respectively) using HYDROPRO program (Garcia De La Torre et al., 2000).

RESULTS AND DISCUSSION

Model quality and structural comparisons

The structures of *P. horikoshii* PdxS in two forms were determined by the molecular replacement method using the hexamer model of PdxS from *G. stearothermophilus* (PDB ID: 1ZNN) (Zhu et al., 2005): (i) the apo form at 2.7 Å resolution and (ii) a binary complex with R5P at 3.1 Å resolution (Fig. 1). The asymmetric unit contains six PdxS monomers for the apo and R5P-bound forms. The refined models gave R_{work}/R_{free} values of 17.3/24.6% for 20-2.7 Å and 18.5/22.7% for 20-3.1 Å data, respectively, for the apo and R5P-bound forms (Table 1). The refined models of the apo and R5P-bound PdxS account for residues 2-316 of monomer A (2-322 of monomers B-F) and 1-333 in each of the six monomers in an asymmetric unit with 344 and 72 water molecules, respectively. Ramachandran plot analysis for the two models showed that 99.37% and 99.65% of the non-glycine residues were in the most favored and allowed regions, and 0.63% and 0.35% of the residues were in disallowed regions (Table 1).

Six monomers of *P. horikoshii* PdxS are almost identical to each other. When monomer A was compared with the other monomers, the r.m.s. deviations averaged over the 5 monomers B-F were 0.26 Å for the 268 Cα atom pairs and 0.31 Å for the 293 Cα atom pairs for the apo and R5P-bound structures, respectively. When monomer A of the apo model was overlapped with monomer A of the R5P-complex model, the r.m.s. deviation was 0.29 Å for the 261 Cα atoms. This suggested that the overall structures of the *P. horikoshii* PdxS apo and R5P complex are similar to each other, except for the movement of α2′ and α8′ toward R5P in the R5P complex form (Fig. 1B). When six monomers of the apo model were overlapped with those of the R5P complex models, the r.m.s. deviation was 0.33 Å for the 1606 Cα atoms. This indicated that there is no significant change in the oligomeric structure of *P. horikoshii* PdxS upon R5P binding.

Table 1. Statistics for data collection and refinement

Data set	Apo	R5P complex
Data collection statistics		
X-ray source	BL-4A (Pohang Light Source)	BL-5 (Photon Factory)
X-ray wavelength (Å)	1.0629	1.00000
Space group	$P2_1$	$P2_1$
a (Å)	59.30	59.16
b (Å)	178.56	179.17
c (Å)	109.23	109.52
β (°)	102.97	102.51
Resolution range (Å)	50-2.61	30-3.1
Total / unique reflections	420,103 / 66,140	320,351 / 39,532
Completeness (%)	100 (100)[a]	98.5 (85.5)[a]
Average I/σ (I)	36.2 (5.4)[a]	8.1 (6.5)[a]
R_{merge}[b] (%)	8.0 (37.3)[a]	6.6 (23.0)[a]
Model refinement statistics		
Resolution range (Å)	20-2.7	20-3.1
R_{work} / R_{free}[c] (%)	17.3 / 24.6	18.5 / 22.7
Number / average *B*-factor (Å^2)		
Protein nonhydrogen atoms	(2,424 + 5 × 2,472) / 52.8	6 × 2,521 / 54.3
Water oxygen atoms	344 / 47.8	72 / 36.5
Ligand (R5P)	None	6 × 13 / 56.2
R.m.s. deviations from ideal		
Bond lengths (Å)	0.009	0.013
Bond angles (°)	1.19	1.63
Protein-geometry analysis		
Ramachandran favored (%)	95.60	96.42
Ramachandran allowed (%)	3.77	3.22
Ramachandran outliers (%)	0.63	0.35

[a]Values in parentheses refer to the highest resolution shell (2.70-2.61 Å for apo and 3.15-3.10 Å for R5P complex, respectively).
[b]$R_{merge} = \Sigma_{hkl}\Sigma_i \mid I_i(hkl) - \langle I(hkl)\rangle \mid / \Sigma_{hkl}\Sigma_i I_i(hkl)_i$, where $I(hkl)$ is the intensity of reflection hkl, Σ_{hkl} is the sum over all reflections, and Σ_i is the sum over i measurements of reflection hkl.
[c]$R = \Sigma_{hkl} \mid |F_{obs}| - |F_{calc}| \mid / \Sigma_{hkl} |F_{obs}|$, where R_{free} was calculated for a randomly chosen 5% of reflections, which were not used for structure refinement and R_{work} was calculated for the remaining.

Overall monomer and quaternary structure

Monomers of *P. horikoshii* PdxS adapt a $(\beta/\alpha)_8$-barrel fold, consisting of 8 parallel β-strands (β1-β8) surrounded with eight α helices (α1-α8) along the polypeptide chain (Figs. 1A and 1C) (Sterner and Hocker, 2005). Modifications to the $(\beta/\alpha)_8$-barrel are a 20-residue N-terminal helix (α1′), which caps the bottom of the β-barrel, helix α2′ inserted between the β2 and α2 loop, the elongated region of helices α6′ and α6″ inserted between helix α6 and strand β7, helix α8′, and additional α-helix (α8″) following helix α8 (Figs. 1A and 1C). The N-terminal helix (α1′) is positioned on the outside of a hexameric ring, whereas the α2′ helix is positioned inside the hexameric ring as in PdxS homologs from *B. subtilis* and *G. stearothermophilus* (Strohmeier et al., 2006; Zhu et al., 2005). The asymmetric unit of *P. horikoshii* PdxS crystals for the apo and R5P-bound forms contains a hexamer (Fig. 2). In the R5P-bound structure of *P. horikoshii* PdxS, all six subunits are bound with R5P.

The overall monomer and hexamer structures of *P. horikoshii* PdxS are similar to those of other PdxS proteins (Fig. 1C) (Guedez et al., 2012; Strohmeier et al., 2006; Zhang et al., 2010; Zhu et al., 2005). When monomer A of the *P. horikoshii* PdxS apo model was overlapped with monomer A of the other PdxS proteins (PdxS homologs from *B. subtilis*, *G. stearothermophilus*, *S. cerevisiae*, *M. jannaschii*, and *P. berghei*), the r.m.s. deviations were 0.42 Å, 0.42 Å, 0.41 Å, 0.46 Å, and 0.62 Å for 195, 189, 207, 259, and 213 Cα atoms, respectively. The significant structural difference in *P. horikoshii* PdxS is the 37 amino-acid insertion between α6′ and α6″ (Figs. 1C and 3). *P. horikoshii* PdxS has longer α6′ and α6″, which are connected by a long loop between them (Figs. 1C and 3). When the hexameric PdxS (apo form) from *P. horikoshii* was overlapped with those of other PdxS proteins (PdxS homologs from *B. subtilis*, *G. stearothermophilus*, *S. cerevisiae*, and *M. jannaschii*, the r.m.s. deviations were 0.92 Å, 1.14 Å, 0.73 Å, and 0.71 Å for 1280, 1267, 1296, and 1586 Cα atoms, respectively (Guedez et al., 2012; Strohmeier et al., 2006; Zhu et al., 2005).

Oligomeric state in solution

The elongated α6 and inserted α6′ and α6″ regions are required for dodecamer formation (Strohmeier et al., 2006; Zein

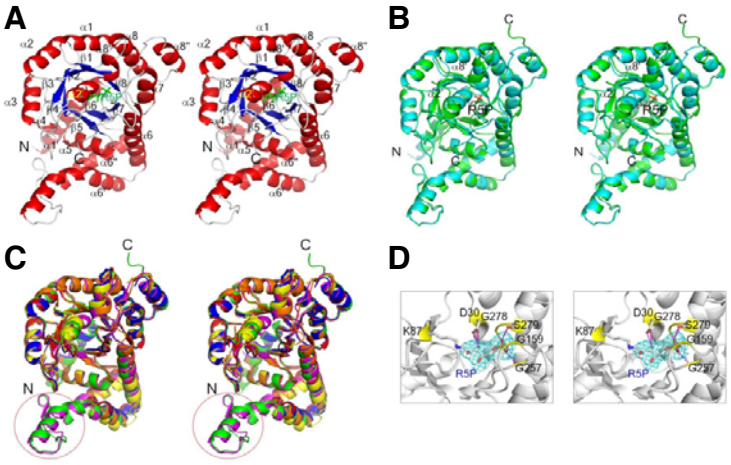

Fig. 1. Monomer structure and R5P binding mode of *P. horikoshii* PdxS. (A) Stereo ribbon diagram of the monomer (R5P complex). α-Helices, β-strands, and loops are colored in red, blue, and gray, respectively. All figures except Fig. 3 were drawn using PyMOL software (The PyMOL Molecular Graphics System, http://www.pymol.org). Figure 3 was drawn with ClustalX (Thompson et al., 1997) and GeneDoc (Nicholas et al., 1997). (B) Superposition of the monomeric apo form (green) with the R5P complex form (cyan) of *P. horikoshii* PdxS. (C) Structural comparison of *P. horikoshii* PdxS and its homologs in stereo. Superposition of *P. horikoshii* PdxS (PDB ID 4FIQ, colored in green) with YaaD from *B. subtilis* (PDB ID code 2NV1, colored in blue), PdxS from *G. stearothermophilus* (PDB ID code 1ZNN, colored in red), SNZ1 from *S. cerevisiae* (PDB ID code 3O06, colored in yellow), PdxS from *M. jannaschii* (PDB ID code 2YZR, colored in magenta), and Pdx1 from *P. berghei* (PDB ID code 4ADT, colored in orange). The insertion region (Tyr199-Ile235) is enclosed by the dotted circle (red). (D) R5P binding mode of *P. horikoshii* PdxS in stereo. Side chains of the residues lining the active site are shown. Red dotted lines depict hydrogen bonds. Omit electron density maps around the R5P molecule are superimposed (3.0 sigma).

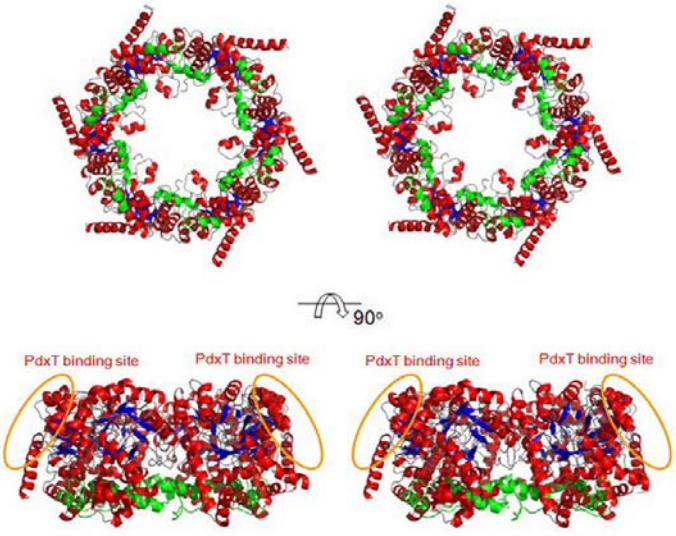

Fig. 2. Stereo ribbon diagram of the hexamer structure of *P. horikoshii* PdxS (R5P complex). α-Helices, β-strands, and loops are colored in red, blue, and gray, respectively. The insertion regions (Tyr199- Ile235) of each monomer are colored in green. Stereo ribbon diagrams of the hexamer (R5P complex) rotated by 90° around the indicated axis in comparison to the upper figure are drawn below.

et al., 2006; Zhu et al., 2005) and the hexamer-hexamer interface containing these regions (α6, α6′, and α6″) showed a complementary shape between the two hexamers (Zhu et al., 2005). *S. cerevisiae* Snz1 has been shown to exist as a hexamer in solution, and it has been suggested that a small insertion (Lys177) between α6 and α6′ prevents dodecamer formation (Neuwirth et al., 2009). This small insertion induces a conformational difference of the elongated and inserted regions α6, α6′, and α6″, respectively, with those of *B. subtilis* Pdx1 inducing a steric clash on the hexamer-hexamer interface (Neuwirth et al., 2009). In case of *P. horikoshii* PdxS, the inserted regions α6′ and α6″ are longer than those in other PdxS homologs (Figs. 1C and 3). To check whether this insertion interferes sterically with dodecamer formation, the *P. horikoshii* PdxS monomer was superimposed on the dodecamer structure of *B. subtilis* Pdx1 (Fig. 4A) (Strohmeier et al., 2006). Indeed, the superimposed *P. horikoshii* PdxS monomer showed a steric clash with the neighboring subunit of *B. subtilis* Pdx1 (Fig. 4A). The longer inserted region (37 amino acids) appeared to contribute to the loss of shape complementarity on the hexamer-hexamer interface (Strohmeier et al., 2006; Zein et al., 2006; Zhu et al., 2005).

The hexamer-hexamer interface of *G. stearothermophilus* PdxS and *B. subtilis* Pdx1 consists of the α4, α5, α6, α6′, and α6″ regions (Strohmeier et al., 2006; Zein et al., 2006; Zhu et al., 2005), and hydrogen bonding interactions exist at the α6 and α6′ helices of the hexamer-hexamer interface (Table 2). Among these hydrogen bonding pairs, a hydrogen bond between Arg165 (Arg171 in *P. horikoshii* PdxS) and Asp180 (Glu186 in *P. horikoshii* PdxS) commonly exists in *G. stearothermophilus* PdxS and *B. subtilis* Pdx1, and two residues, Arg165 and Asp180, in both *G. stearothermophilus* PdxS and *B. subtilis* Pdx1, are conserved (Figs. 3 and 4A). In the case of *P. horikoshii* PdxS, the constitution of the hexamer-hexamer interface might be changed to the C-terminal of the α6, α6′, and α6″ regions because of the long inserted region (Figs. 3 and 4A). The conserved Arg171 residue of *P. horikoshii* PdxS, which is

Table 2. Hydrogen bonding pairs at the hexamer-hexamer interface

B. subtilis YaaD (residues in *P. horikoshii* PdxS)	*G. stearothermophilus* PdxS (residues in *P. horikoshii* PdxS)
Glu113 (Phe119) and Thr184 (Gly190)	Arg165 (Arg171) and Asp180 (Glu186)
Asn117 (Tyr123) and Glu179 (Asp185)	Arg172 (Arg178) and Ser178 (Thr184)
Arg165 (Arg171) and Asp180 (Glu186)	Lys173 (Leu179) and Asn176 (Arg182)

Table 3. Hydrogen bonds (Å) between R5P and PdxS

R5P	*P. horikoshii* PdxS	*P. berghei* Pdx1
O1	Lys87 NZ (linked)	Lys84 NZ (linked)
O2		Asp27 OD2 (2.7)
O3	Asp30 OD1 (3.1)	
	Asp30 OD2 (3.1)	
O1P	Gly159 N (2.9)	Gly156 N (2.7)
	Gly257 N (2.8)	Gly217 N (3.0)
O2P	Ser279 N (2.7)	Ser239 N (2.8)
	Ser279 OG (2.8)	Ser239 OG (2.8)
O3P	Gly278 N (3.1)	Gly238 N (2.7)

The cutoff distance between the pairs of hydrogen-bonded heavy atoms is 3.2 Å.

Fig. 3. Multi-alignment of *P. horikoshii* PdxS (UniProtKB/Swiss-Prot accession No. O59080) against PdxS homologs from *B. subtilis* (UniProtKB/Swiss-Prot accession No. P37527), *G. stearothermophilus* (UniProtKB/Swiss-Prot accession No. Q5L3Y2), *M. jannaschii* (UniProtKB/Swiss- Prot accession No. Q58090), *S. cerevisiae* (UniProtKB/ Swiss-Prot accession No. Q03148), and *P. berghei* (UniProtKB/Swiss-Prot accession No. Q4Z0E8). Secondary structure elements were assigned by PyMOL and every twentieth residue is marked by a black dot. Arrows above the sequences denote α-helices and cylinders β-strands. The 37 amino acid insertion region (Tyr199-Ile235) of *P. horikoshii* PdxS and *M. jannaschii* PdxS are enclosed by a blue box. Red triangles above the sequences indicate the residues that interact with the R5P molecule. Blue diamonds above the sequences indicate the conserved residues that form hydrogen bonds on the hexamer-hexamer interface of *G. stearo-thermophilus* PdxS and *B. subtilis* Pdx1.

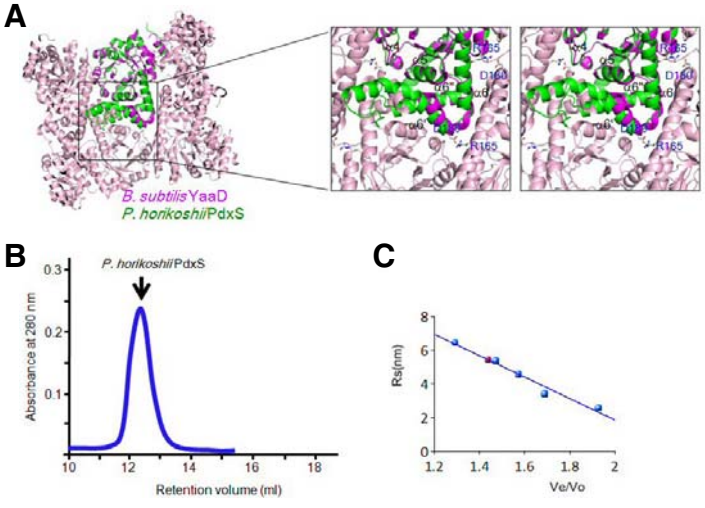

Fig. 4. Oligomeric state of *P. horikoshii* PdxS in solution. (A) Superposition of *P. horikoshii* PdxS (colored in green) and *B. subtilis* YaaD (colored in magenta) on the *B. subtilis* YaaD dodecamer (colored in light magenta, PDB ID code 2NV1). Arg165 and Asp180 in *B. subtilis* YaaD are shown as sticks. (B, C) Gel filtration analysis of *P. horikoshii* PdxS. Molecular weight markers (Sigma, catalog no. MWGF1000-1KT) containing apoferritin, β-amylase, alcohol dehydrogenase, albumin, and carbonic anhydrase were used to generate the standard curve. The position of *P. horikoshii* PdxS is marked as a red dot.

located on α6, might be inaccessible to the other hexamer because of the long insertion (Figs. 3 and 4A).

To analyze the oligomeric states of *P. horikoshii* PdxS in solution, we performed analytical gel filtration with a Superdex 200

(10/300) column (Figs. 4B and 4C). Using the gel-filtration data, the Stokes radius of *P. horikoshii* PdxS in solution was estimated to be 5.43 nm, which is similar to the calculated Stokes radius (5.27 nm) of the hexameric structure of *P. horikoshii* PdxS (Figs. 4B and 4C). As a reference, the calculated Stokes radius of the dodecameric structure of *B. subtilis* Pdx1 is 6.04 nm. This result strongly suggests that *P. horikoshii* PdxS exists as a hexamer in solution, as is predicted from the crystal structure of *P. horikoshii* PdxS.

Binding mode of R5P

In the structure of the R5P complex of *P. horikoshii* PdxS, R5P molecules are clearly defined by their electron density and are bound in the active sites of all six chains of the homohexamer (Fig. 1D). Lys87 forms a Schiff base with the C1 carbonyl of R5P and stretches across the bottom (the N-terminal end of the β-barrel) (Fig. 1D). Asp30 forms a hydrogen bond with the C3 hydroxyl group of R5P (3.1 Å). Phosphate oxygen atoms of R5P form hydrogen bonds with amide nitrogen atoms of Gly159, Gly257, Gly278, and Ser279 (2.9 Å, 2.8 Å, 3.1 Å, and 2.7 Å, respectively) (Fig. 1D and Table 3). All of the R5P binding site residues (Lys87, Asp30, Gly159, Gly257, Gly278, and Ser279) are conserved among the PdxS homologs (Fig. 3), and the binding mode of R5P in the *P. horikoshii* PdxS structure is similar to that in the R5P-bound structure of *P. berghei* Pdx1 (Guedez et al., 2012).

ACKNOWLEDGMENTS

The author wishes to thank the staff at beamline BL-4A of Pohang Light Source and beamline BL5 of Photon Factory (Japan) for their assistance during the X-ray experiments. This study was supported by the National Research Foundation of Korea (NRF) grant funded by the Korean government (Ministry of Education, Science and Technology) (grant no. 2012-0004085) and by the Research Program 2012 of Kookmin University to HHL. This work was also supported by the Seoul R&BD program (ST100072) to HHL and by the National Research Foundation of Korea (NRF) grant funded by the Korean government (2011-0013663) to HJY.

REFERENCES

Belitsky, B.R. (2004). Physical and enzymological interaction of Bacillus subtilis proteins required for *de novo* pyridoxal 5′-phosphate biosynthesis. J. Bacteriol. *186*, 1191-1196.

Bender, D.A. (1989). Vitamin B_6 requirements and recommendations. Eur. J. Clin. Nutr. *43*, 289-309.

Brünger, A.T., Adams, P.D., Clore, G.M., DeLano, W.L., Gros, P., Grosse-Kunstleve, R.W., Jiang, J.S., Kuszewski, J., Nilges, M., Pannu, N.S., et al. (1998). Crystallography & NMR system: A new software suite for macromolecular structure determination. Acta Crystallogr. D Biol. Crystallogr. *54*, 905-921.

Cane, D.E., Du, S., Robinson, J.K., Hsiung, Y., and Spenser, I.D. (1999). Biosynthesis of vitamin B_6: enzymatic conversion of 1-deoxy-D-xylulose-5-phosphate to pyridoxol phosphate. J. Am. Chem. Soc. *121*, 7722-7723.

Chung, K.R., Jenns, A.E., Ehrenshaft, M., and Daub, M.E. (1999). A novel gene required for cercosporin toxin resistance in the fungus *Cercospora nicotianae*. Mol. Gen. Genet. *262*, 382-389.

Dong, Y.X., Sueda, S., Nikawa, J., and Kondo, H. (2004). Characterization of the products of the gene SNO1 and SNZ1 involved in pyridoxine synthesis in *Saccharomyces cerevisiae*. Eur. J. Biochem. *271*, 745-752.

Ehrenshaft, M., Bilski, P., Li, M.Y., Chignell, C.F., and Daub, M.E. (1999). A highly conserved sequence is a novel gene involved in de novo vitamin B_6 biosynthesis. Proc. Natl. Acad. Sci. USA *96*, 9374-9378.

Eliot, A.C., and Kirsch, J.F. (2004). Pyridoxal phosphate enzymes: Mechanistic, structural, and evolutionary considerations. Annu. Rev. Biochem. *73*, 383-415.

Fitzpatrick, T.B., Amrhein, N., Kappes, B., Macheroux, P., Tews, I., and Raschle, T. (2007). Two independent routes of *de novo* vitamin B_6 synthesis: not that different after all. Biochem. J. *407*, 1-13.

Garcia De La Torre, J., Huertas, M.L., and Carrasco, B. (2000). Calculation of hydrodynamic properties of globular proteins from their atomic-level structure. Biophys. J. *78*, 719-730.

Guedez, G., Hipp, K., Windeisen, V., Derrer, B., Gengenbacher, M., Bottcher, B., Sinning, I., Kappes, B., and Tews, I. (2012). Assembly of the eukaryotic PLP-synthase complex from *Plasmodium* and activation of the Pdx1 Enzyme. Structure *20*, 172-184.

Jones, T.A., Zou, J.Y., Cowan, S.W., and Kjeldgaard, M. (1991). Improved methods for the building of protein models in electron density maps and the location of errors in these models. Acta Cryst. A *47*, 110-119.

Laber, B., Maurer, W., Scharf, S., Stepusin, K., and Schmidt, F.S. (1999). Vitamin B_6 biosynthesis: formation of pyridoxine 5′-phosphate from 4-(phosphohydroxy)-L-threonine and 1-deoxy-D-xylulose-5-phosphate by PdxA and PdxJ protein. FEBS Lett. *449*, 45-48.

Lee, H.H. (2012). High-resolution structure of shikimate dehydrogenase from Thermotoga maritima reveals a novel tightly closed conformation. Mol. Cells *33*, 229-233.

Neuwirth, M., Strohmeier, M., Windeisen, V., Wallner, S., Deller, S., Rippe, K., Sinning, I., Macheroux, P., and Tews, I. (2009). X-ray crystal structure of *Saccharomyces cerevisiae* Pdx1 provides insights into the oligomeric nature of PLP synthases. FEBS Lett. *583*, 2179-2186.

Nicholas, K.B., Nicholas Jr., H.B., and Deerfield II, D.W. (1997). GeneDoc: analysis and vsualization of genetic variation. EMBnet News *4*, 14.

Osmani, A.H., May, G.S., and Osmani, S.A. (1999). The extremely conserved pyroA gene of *Aspergillus nidulans* is required for pyridoxine synthesis and is required indirectly for resistance to photosensitizers. J. Biol. Chem. *274*, 23565-23569.

Percudani, R., and Peracchi, A. (2003). A genomic overview of pyridoxal-phosphate-dependent enzymes. EMBO Rep. *4*, 850-854.

Sterner, R., and Hocker, B. (2005). Catalytic versatility, stability, and evolution of the (betaalpha)8-barrel enzyme fold. Chem. Rev. *105*, 4038-4055.

Strohmeier, M., Raschle, T., Mazurkiewicz, J., Rippe, K., Sinning, I., Fitzpatrick, T.B., and Tews, I. (2006). Structure of a bacterial pyridoxal 5′-phosphate synthase complex. Proc. Natl. Acad. Sci. USA *103*, 19284-19289.

Tambasco-Studart, M., Titiz, O., Raschle, T., Forster, G., Amrhein, N., and Fitzpatrick, T.B. (2005). Vitamin B_6 biosynthesis in higher plants. Proc. Nat. Acad. Sci. USA *102*, 13687-13692.

Thompson, J.D., Gibson, T.J., Plewniak, F., Jeanmougin, F., and Higgins, D.G. (1997). The CLUSTAL_X windows interface: flexible strategies for multiple sequence alignment aided by quality analysis tools. Nucleic Acids Res. *25*, 4876-4882.

Yoon, H.J., Kang, J.Y., Mikami, B., Lee, H.H., and Suh, S.W. (2011). Crystal structure of phosphopantetheine adenylyltransferase from *Enterococcus faecalis* in the ligand-unbound state and in complex with ATP and pantetheine. Mol. Cells *32*, 431-435.

Yoon, J.Y., Park, C.R., Lee, H.H., and Suh, S.W. (2012). Overexpression, crystallization and preliminary X-ray crystallographic analysis of pyridoxal biosynthesis lyase PdxS from *Pyrococcus horikoshii*. Acta Cryst. Sect. F Struct. Biol. Cryst. Commun. *68*, 440-442.

Zein, F., Zhang, Y., Kang, Y.N., Burns, K., Begley, T.P., and Ealick, S.E. (2006). Structural insights into the mechanism of the PLP synthase holoenzyme from *Thermotoga maritima*. Biochemistry *45*, 14609-14620.

Zhang, X., Teng, Y.B., Liu, J.P., He, Y.X., Zhou, K., Chen, Y., and Zhou, C.Z. (2010). Structural insights into catalytic mechanism of the yeast pyridoxal 5-phosphate synthase Snz1. Biochem. J. *432*, 445-450.

Zhu, J., Burgner, J.W., Harms, E., Belitsky, B.R., and Smith, J.L. (2005). A new arrangement of (beta/alpha)8 barrels in the synthase subunit of PLP synthase. J. Biol. Chem. *280*, 27914-27923.